Chemical Engineering Journal 146 (2009) 259–265

Contents lists available at ScienceDirect

Chemical Engineering Journal

journal homepage: www.elsevier.com/locate/cej

Numerical analysis of water vapor nucleation on $PM_{2.5}$ from municipal solid waste incineration

Fengxian Fan [a,b,*], Linjun Yang [b], Jinpei Yan [b], Zhulin Yuan [b]

[a] School of Power Engineering, University of Shanghai for Science and Technology, No. 516, Jungong Road, Shanghai 200093, China
[b] Thermal Energy Research Institute, Southeast University, Nanjing 210096, China

ARTICLE INFO

Article history:
Received 23 December 2007
Received in revised form 24 May 2008
Accepted 9 June 2008

Keywords:
$PM_{2.5}$ from MSWI
Vapor nucleation
Nucleation capability
Numerical simulation

ABSTRACT

Vapor nucleation on $PM_{2.5}$ from MSWI (municipal solid waste incineration) was modeled combined with the wetting abilities, compositions and surface characteristics of the particles. Nucleation characteristics of the fine particles were numerically studied. Results show that when the mass fraction of each salt is constant the free energy barrier of embryo formation is not influenced by the total mass of soluble salts in the particle. While the total mass of soluble salts does not change, the free energy barrier changes remarkably with the compositions of the soluble salts in the particle. It is also found that the free energy barrier decreases with roughness of particle surfaces. Simulation results of the nucleation rate and the critical nucleation saturation indicate that both the compositions of the soluble salts and the surface roughness dominate the activation of the $PM_{2.5}$ from MSWI.

1. Introduction

A number of researches have correlated ambient particulate matter that is less than 2.5 μm in aerodynamic diameter ($PM_{2.5}$) with negative impacts on human health and the environment [1,2]. Conventional particulate removal devices are generally less efficient in collecting $PM_{2.5}$ particles generated during fuel combustion. Thus, large amounts of emissions from combustion become a significant source of $PM_{2.5}$ suspended in the air [3,4]. For these reasons, how to effectively remove the $PM_{2.5}$ particles has received urgent concern in the research fields of energy and environment. Water vapor heterogeneous condensation on the surfaces of the $PM_{2.5}$ is able to make the particles grow big enough to remove in scrubber columns, for example, Venturi scrubber [5]. The process of particle enlargement by heterogeneous condensation can be divided into two steps. First, the particles have to be activated, which is called nucleation or activation. Secondly, the nuclei grow to droplets by condensation of vapor. In the case of heterogeneous condensation, degrees of supersaturation that have determining influences on the effect of particle activation are necessary. In order to predict the critical saturation numerically, one should consider theories of heterogeneous nucleation.

Efforts have been made on heterogeneous nucleation theory, since Fletcher [6] presented a theory of water nucleation on insoluble spherical particles with uniform surfaces for the first time. Gorbunov and Hamilton [7] and Gorbunov et al. [8] developed a theory of water nucleation on aerosol particles which consist of both soluble non-volatile substances and insoluble cores. Lazaridis et al. [9] examined the effect of surface roughness of insoluble solid particles on their activation capability.

The physical and chemical properties of particles considerably affect heterogeneous characteristics. However, the particles from different sources (oil burning, coal combustion, waste incineration) differ greatly in compositions, surface characteristics and consequent wetting abilities. Researchers studied the properties of fly ashes from MSWI. They drew a conclusion that the fly ashes from MSWI appear as rough, porous particles and contain 17–27% soluble salts which are mainly $CaCl_2$, NaCl, and KCl [10–12]. We have examined the particles that withdraw from fly ashes collected by an electrostatic precipitator, using a LEO 1530 VP Series Scanning Electron Microscope (SEM). The morphology information of the particles observed is given in Fig. 1. The particles show signs of stretching, fracturing, or other irregularities with high surface-to-volume ratios. It is also noted that many particles examined appear to be primarily sphere in shape.

In this paper, numerical analyses are conducted with suitable theories to study the nucleation characteristics of the $PM_{2.5}$ from MSWI, including the free energy of embryo formation, the nucleation rate and the critical nucleation saturation. We show the impacts of the particle properties on the nucleation abilities and discuss the levels of saturations which are required to activate the $PM_{2.5}$ particles that are difficult to remove by conventional particulate removal devices.

* Corresponding author. Tel.: +86 21 55272320.
E-mail addresses: fanfengxian@tom.com, fanfengxian@hotmail.com (F. Fan).

1385-8947/$ – see front matter © 2008 Elsevier B.V. All rights reserved.
doi:10.1016/j.cej.2008.06.009

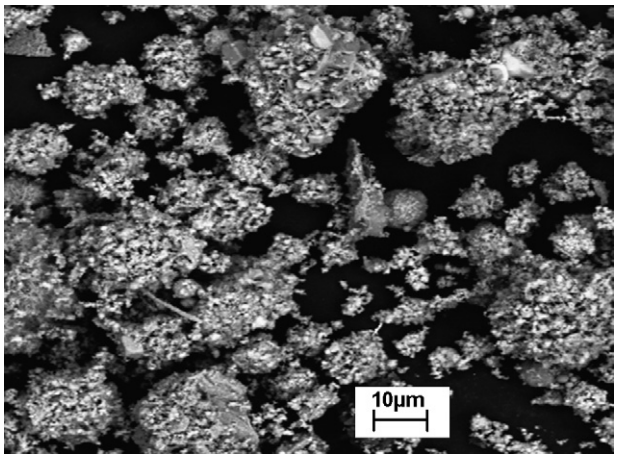

Fig. 1. Morphology of $PM_{2.5}$ from municipal solid waste incineration.

2. Description of the simulation model

2.1. Wetting ability of rough surface

We tested the wetting ability of the $PM_{2.5}$ from MSWI using the Washburn penetration pressure method. In this method, the particle contact angle is measured by the capillary penetration of liquid technique and is calculated by the Washburn equation. For a detailed account of Washburn penetration method, one is referred to the publication of Subrahmanyam et al. [13]. We found that the contact angle between the particles and water is 76.19°. Since surfaces of $PM_{2.5}$ from MSWI appear to be rough and heterogeneous as mentioned in Section 1, it is reasonable to expect that the surface roughness can influence the wetting ability of the particles. Chow [14,15] viewed the rough surfaces as self-affine fractal surfaces and found that roughness enhances wetting. Here we adopt Chow's approach to study the impacts of surface roughness on the change of local contact angle.

Let us consider an embryo formation from a gas phase on an ideal smooth solid surface, the contact angle is determined by Young equation:

$$\sigma_{gs} - \sigma_{es} = \sigma_{eg} \cos\theta_0 \tag{1}$$

where σ_{gs}, σ_{es} and σ_{eg} are the interfacial tensions of the gas–solid, embryo–solid and embryo–gas interface respectively, and θ_0 is the contact angle of the smooth surface.

For rough surfaces, the spatial coordinates (x, y) are introduced into the Young equation to generalize it as [14,15]

$$\sigma_{gs} - \sigma_{es} = \sigma_{eg} \cos\theta(x,y) = \sigma_{eg} \cos[\theta(x,y)_0 - \phi(x,y)] \tag{2}$$

where θ is the local contact angle of the rough surface, and ϕ is the decrease of contact angle due to the surface roughness.

According to Taylor expansion, $\cos[\theta(x,y)_0 - \phi(x,y)]$ can be written as

$$\cos[\theta(x,y)_0 - \phi(x,y)] = \cos\ \theta(x,y)_0 + \sin\theta(x,y)_0\phi(x,y) + \dots \tag{3}$$

For a small ϕ, we get

$$\frac{\cos[\theta(x,y)_0 - \phi(x,y)]}{\cos\ \theta(x,y)_0} \approx 1 + \tan\theta(x,y)_0\phi(x,y) \tag{4}$$

A fractal called self-affine is suitable in the description of anisotropic rough surfaces. The self-affine fractal is statistically invariant under an anisotropic dilatation. This is different from the self-similar fractal which is invariant under isotropic scale transformation and is suitable in description of the isotropic structure. Using the conception of self-affine fractal and taking the spatial average, it gives [15]

$$\bar{\phi} = \frac{C_\alpha \sigma}{\xi} \tag{5}$$

where C_α is a non-dimensional correction factor, including the effect of the correlated noise due to fluctuations; and σ is the standard deviation which is related to the fluctuation normal to the surface and the correlation length ξ. In the case where there is no correlated noise $C_\alpha = 1$, and for a smooth surface $\xi = 0$.

From Eqs. (4) and (5), we obtain

$$\frac{\cos[\theta(x,y)_0 - \phi(x,y)]}{\cos\ \theta(x,y)_0} \approx 1 + \tan\theta(x,y)_0 \frac{C_\alpha \sigma}{\xi} \tag{6}$$

Eq. (6) enables us to determine the effect of surface roughness on the local contact angle.

2.2. Heterogeneous nucleation model

Theoretical models of heterogeneous nucleation for particulates have been limited to spherical particles due to lack of knowledge about interactions between the liquid nucleating embryo and the solid particles that have irregular shapes and complex surfaces. The nucleation theory developed by Gorbunov and Hamilton [7] and Gorbunov et al. [8] allows calculating free energy of water droplet formation on a particle which contains both soluble and insoluble non-volatile species. We will use this theory to estimate the nucleation characteristics of the $PM_{2.5}$ from MSWI. The physical model of the theory is shown in Fig. 2 [7,8].

Referring to Fig. 2 we can see that the $PM_{2.5}$ is simplified as a particle consisting of an insoluble core and soluble salts. This simplification is rather crudely taken into account in the real particle shape and surface of $PM_{2.5}$ from MSWI. However, a rigorous theoretical model must be based on more complete mathematical description of surface properties and shapes of particles than is currently possible and must be deferred to future studies.

In the case of heterogeneous nucleation illustrated in Fig. 2, the Gibbs free energy ΔG as a result of the embryo formation from water vapor under a constant pressure and temperature can be expressed as a function of the nucleating embryo radius r_e [7,8]:

$$\Delta G(r_e) = \int_0^{r_e} R_g T \ln\left(\frac{a_w}{S_w}\right) \frac{dn_w}{dr}\, dr + \int_0^{r_e} \sigma_{eg} \frac{ds_{eg}}{dr}\, dr + \int_0^{r_e} (\sigma_{es} - \sigma_{gs}) \frac{ds_{es}}{dr}\, dr \tag{7}$$

where R_g is the universal gas constant, T is the temperature, a_w is the water activity in the embryo, S_w is the degree of saturation of water vapor, n_w is a number of moles of water in an embryo, s_{eg} and s_{es} are the areas of embryo–gas and embryo–solid interfaces respectively, and r is an integration variable.

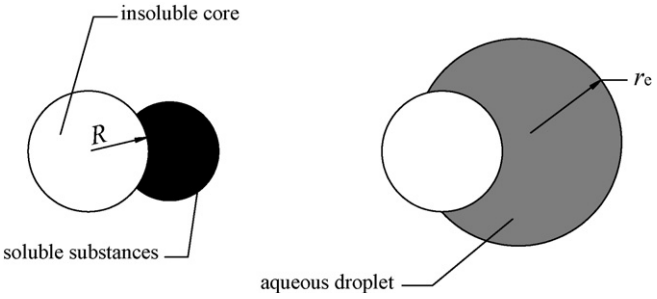

Fig. 2. Vapor nucleation on a particle containing both soluble and insoluble substances.

The expressions for ds_{eg}/dr and ds_{es}/dr can be obtained from Fig. 2:

$$\frac{ds_{eg}}{dr} = 2\pi R\left[\frac{2}{X}\left(1+\frac{1}{g}\right) - \frac{m}{g} + \frac{X-m}{g^3}(1-mX)\right] \tag{8}$$

$$\frac{ds_{es}}{dr} = \frac{2\pi RX^2}{g}\left[1-\left(\frac{X-m}{g}\right)^2\right] \tag{9}$$

$$V = \frac{\pi R^3}{3} \times \left[\frac{2}{X^3} - 2 + 3\frac{(1-mX)}{gX^3} + 3\frac{(X-m)}{g} - \left(\frac{1-mX}{gX}\right)^3 - \left(\frac{X-m}{g}\right)^3\right] \tag{10}$$

where R is the radius of the insoluble core of the solid particle, m is the cosine of the contact angle θ, V is the embryo volume, and X and g are expressed as

$$X = \frac{R}{r} \tag{11}$$

$$g = (1 + X^2 - 2mX)^{1/2} \tag{12}$$

Meanwhile, from the mass and density of the embryo we get:

$$V = \frac{(n_w M_{ww} + \sum_{i=1}^{I} n_{si} M_{wsi})}{\rho(x_w)} \tag{13}$$

$$x_w = \frac{n_w}{(n_w + \sum_{i=1}^{I} n_{si})} \tag{14}$$

where M_{ww} is the molecular weight of water, M_{wsi} and n_{si} are the molecular weight and number of moles of soluble component i in the particle respectively, I is the number of soluble components, and $\rho(x_w)$ is the density of the embryo solution, which depends on the embryo size, the mass fraction and the compositions of the soluble salts.

The expression for dV/dr can be derived from Eq. (10):

$$\frac{dV}{dr} = \pi R^2\left\{\frac{2}{X^2} - \frac{(1-m^2)X^2}{g^5} + 2\frac{(1-mX)}{gX^2} + \frac{(1-m^2)}{g^3} \times \left[1 - \frac{(m-X)(1-mX)X}{g^2}\right]\right\} \tag{15}$$

when the embryo is a saturated solution, dV/dn_w can be written as

$$\frac{dV}{dn_w} = \frac{\sum_{i=1}^{I} S_{si} + 100}{100}\frac{M_{ww}}{\rho_s} \tag{16}$$

where S_{si} is the solubility of the soluble component i, ρ_s is the density of the saturated embryo.

As water vapor continues to condense on the particle, the embryo grows into big ones and therefore may contain more water than salts. For unsaturated solutions, dV/dn_w can be derived:

$$\frac{dV}{dn_w} = \left(1 - \frac{V}{M_{ww}}\frac{d\rho(x_w)}{dx_w}\frac{(1-x_w)}{n_w + \sum_{i=1}^{I} n_{si}}\right)\frac{M_{ww}}{\rho(x_w)} \tag{17}$$

dn_w/dr can be written as

$$\frac{dn_w}{dr} = \frac{(dV/dr)}{(dV/dn_w)} \tag{18}$$

The above equations make it possible to obtain the free energy of embryo formation.

The rate of formation of critical embryos which can then develop into macroscopic droplets is called nucleation rate. It is given by [6]

$$J = 4\pi R^2 K_c \exp\left[-\frac{\Delta G^*}{(kT)}\right] \tag{19}$$

where J is the nucleation rate, K_c is a kinetic coefficient, whose value is somewhat uncertainty and is related to the detailed mechanism of addition of vapor molecules to the particle. The value of K_c usually lies between 10^{28} and 10^{31} m^{-2} s^{-1}. Here we adopt the value 10^{31} m^{-2} s^{-1}, considering the soluble substances may enhance molecule addition. ΔG^* is the free energy barrier of embryo formation, and k is Boltzmann constant whose value is 1.38×10^{-23} J K^{-1}.

2.3. Water activity and interfacial tension

Using only data of corresponding binary subsystems of equal ionic strength, a_w and σ_{eg} can be obtained from the following equations [16,17]:

$$\lg a_w = \sum_i y_i \lg a_{w,i} \tag{20}$$

$$\sigma_{eg} = \sum_i y_i \sigma_{eg,i} \tag{21}$$

where y_i is the ionic strength fraction of component i in the mixed solutions ($y_i = I_i/\sum_i I_i$, I_i is the ionic strength of component i), $a_{w,i}$ and $\sigma_{eg,i}$ are the water activity and the interfacial tension of aqueous solution of component i having the same ionic strength as the mixed solution. Values of water activities are taken from literature [18] and are parameterized as

$$a_{w,i} = 1 - \sum_{j=1}^{4} a_j M_l^j \tag{22}$$

where values of a_j for $CaCl_2$ are $a_1 = 6.21362 \times 10^{-2}$, $a_2 = -2.19473 \times 10^{-2}$, $a_3 = 1.36786 \times 10^{-2}$, and $a_4 = -1.315119 \times 10^{-3}$ respectively; for NaCl, $a_1 = 3.2975479 \times 10^{-2}$, $a_2 = 2.081262 \times 10^{-4}$, $a_3 = 1.85425 \times 10^{-4}$, $a_4 = 0$. M_l is the molality of a solution.

The interfacial tension of the strong electrolyte solution is given by the empirical equation:

$$\sigma_{eg,i}(M_l) = \sigma_{wg} + BM_l \tag{23}$$

The interfacial tensions of $CaCl_2$ aqueous solution are tested via a method of the biggest air-bubble, we get $B = 0.003244$ N m^{-1} per mole of $CaCl_2$ in 1 kg water. For NaCl aqueous solution, we take $B = 0.00162$ N m^{-1} per mole of NaCl in 1 kg water from literature [18].

3. Simulation results and discussion

Combined with the mass fractions and compositions of soluble salts in the $PM_{2.5}$ from MSWI, we assume that the soluble substances shown in Fig. 2 contain two components ($CaCl_2$ and NaCl). Let f_s be the mass fraction of the soluble salts and let f_1 be the mass fraction of $CaCl_2$ contained in soluble salts. The properties of the particles listed in Table 1 are used in the simulation.

In this section the effect of the self-affine factor on the contact angle is studied and the influences of different particle properties on the free energy of embryo formation are investigated. Finally, we work on the nucleation capability of the $PM_{2.5}$ particles to determine the nucleation rate and the critical nucleation saturation.

Table 1
The physical properties of $PM_{2.5}$ from MSWI used in numerical calculation

ρ_p (kg m^{-3})	1,800
f_s	15–30%
f_1	50–65%
$C_\alpha\sigma/\xi$	0–0.1
θ_0 (°)	76.19
T (K)	298.15
P (Pa)	101,325

3.1. Effect of self-affine fractal factor on contact angle

The influence of self-affine fractal factor $C_\alpha\sigma/\xi$ on the decrease of the contact angle ϕ is shown in Fig. 3. Increased values of $C_\alpha\sigma/\xi$ result in increase of ϕ, which is in qualitative agreement with the conclusion drawn by Wang et al. [19]. As can be seen in Fig. 3, ϕ is more than 5.5° for rough surfaces with a self-affine factor of 0.1. This result means that the contact angle of the rough surface θ may decrease several degrees compared with that of the smooth surface θ_0, since $\theta = \theta_0 - \phi$ as it is expressed by Eq. (2). Heterogeneous nucleation characteristics depend strongly on the contact angle of particles. Higher saturations are needed for water vapor to nucleate and condense on the particle with a greater contact angle. Particle roughness is indeed expected because the appearance of rough surface lowers the saturation to enable heterogeneous nucleation due to the decrease of the contact angle.

3.2. Free energy of embryo formation

The free energy of embryo formation under different conditions is numerically analyzed. In this simulation, the diameter of the insoluble core D ($D = 2R$) is chosen to be 2 μm. The calculation results are given in Figs. 4–7.

Fig. 4 shows the influence of the water vapor saturation S_w on the relative free energy of embryo formation $\Delta G/(kT)$. Fig. 4(a) clearly presents the initial stage of nucleating process in which the embryo is only several nanometers, whereas Fig. 4(b) illustrates the changes of free energy with the embryo radius in further condensational process. At the beginning, the free energy increases, but it decreases monotonously after passing through the maximum. The maximum free energy shown in Fig. 4(a) represents the free energy barrier of embryo formation ΔG^*. In the case of heterogeneous condensation the embryo has to pass through the free energy barrier in order to achieve substantial vapor condensation to form the big-sized droplet. This indicates that the $PM_{2.5}$ particles will be enlarged to relatively larger particles by vapor condensation if the barrier ΔG^* is not very high. From Fig. 4, it is found that

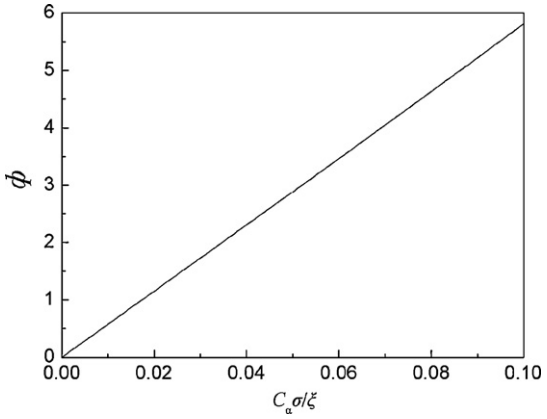

Fig. 3. Influence of self-affine fractal factor on change of contact angle.

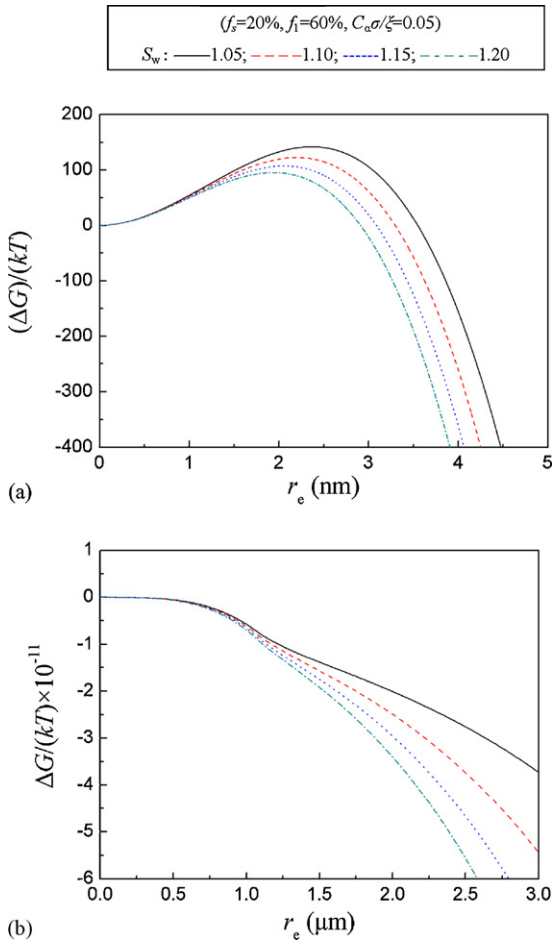

Fig. 4. Influence of water vapor saturation on free energy of embryo formation. (a) Initial stage of nucleation, (b) process of embryo growth.

increase of S_w leads to decrease of free energy barrier. Therefore, the $PM_{2.5}$ particles are more likely to activate at higher degrees of saturation.

Fig. 5 gives the influence of the mass fraction of soluble salts f_s on the relative free energy of embryo formation $\Delta G/(kT)$. The salts are not able to be fully dissolved in an embryo with a radius less than 5 nm, thus the embryo formed is a saturated solution. In this case the physical and chemical properties, such as the density, the water activity and the interfacial tension, are independent of the total mass of salts in the initial stage of nucleation. Therefore, the total mass of the soluble salts has no effect on the free energy barrier of embryo formation and the lines coincide with each other as can be seen from Fig. 5(a). After it passes through the free energy barrier, more water condenses on the embryo. As a result, the embryo becomes an unsaturated solution which contains more water than salts. Since the total mass of salts in the particles is different, the concentration of the embryos of the same size differs from each other. Therefore, the free energy decreases with the increase of the mass fraction of soluble salts when the size of the embryo is greater than 1 μm as can be seen from Fig. 5(b). Nevertheless, the activation and growth of the $PM_{2.5}$ particles do not depend on the mass fraction of soluble salts while keeping the size of insoluble core D and the mass fraction of $CaCl_2$ in the soluble salts f_1 unchanged, because the free energy barrier of embryo formation determines the nucleation rate and the subsequent critical saturation on the particle with a given diameter as implied in Eq. (19).

Fig. 6 presents the influence of the mass fraction of $CaCl_2$ in soluble salts f_1 on the relative free energy of embryo formation $\Delta G/(kT)$. The free energy barrier of embryo formation ΔG^* decreases remarkably as the mass fraction of $CaCl_2$ increases from 50 to 65%. The trend of ΔG changing with the mass fraction of $CaCl_2$ in Fig. 6(b) is similar to that of the initial stage of nucleation shown in Fig. 6(a). Increased values of mass fraction of $CaCl_2$ result in increase in the density and surface tension of embryo, but decrease in the water activities. On one hand, increase of surface tension can increase ΔG; on the other hand, decrease of water activity makes ΔG decrease. The impacts of multi-factor result in the curves as shown in Fig. 6. Since the free energy decreases with the increase of the mass fraction of $CaCl_2$ in the soluble salts, we can conclude that the water activity of the embryo solution plays an important role in the nucleation process. It is easier for $PM_{2.5}$ containing more $CaCl_2$ to activate and grow when subjected to supersaturated vapor conditions. If a greater amount of $CaCl_2$ is present in soluble salts at the surface of a $PM_{2.5}$ particle, nucleation will take place at a lower degree of saturation.

Fig. 7 illustrates the influence of the self-affine fractal factor $C_\alpha\sigma/\xi$ on the relative free energy of embryo formation $\Delta G/(kT)$. As can be seen from Fig. 7(a), the free energy barrier of embryo formation ΔG^* decreases with the increase of self-affine fractal factor $C_\alpha\sigma/\xi$. Because the embryo formation relates to direct addition of water vapor to the particle surface in the initial stage of nucleation, surface roughness has an obvious impact upon the nucleation free energy as well as the free energy barrier. As an

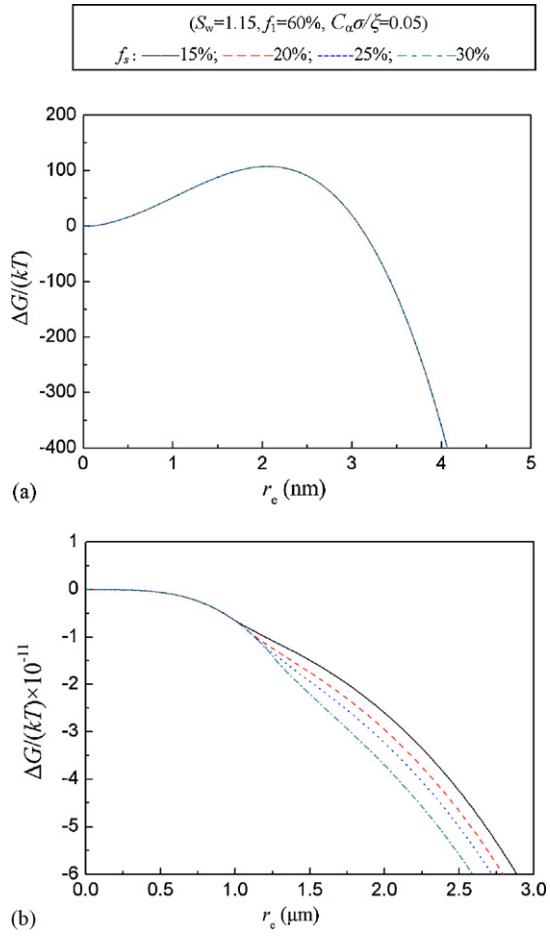

Fig. 5. Influence of mass fraction of soluble salts on free energy of embryo formation. (a) Initial stage of nucleation, (b) process of embryo growth.

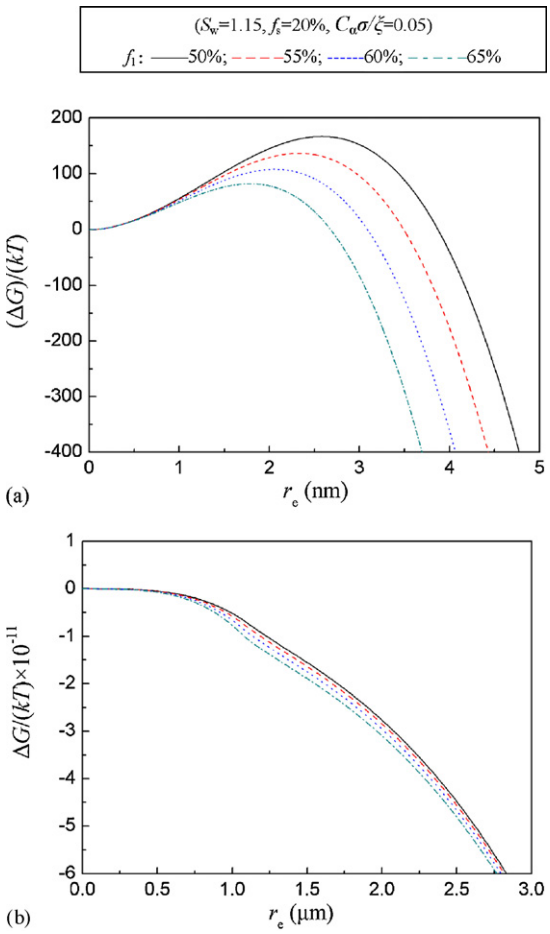

Fig. 6. Influence of mass fraction of $CaCl_2$ on free energy of embryo formation. (a) Initial stage of nucleation, (b) process of embryo growth.

embryo grows to a bigger size like hundreds or thousands of nanometers, the rough surface are covered with the nucleating liquid. The embryo growth in this stage refers to water vapor addition to the interface of gas–embryo, therefore ΔG is not influenced by the surface roughness, as it is shown in Fig. 7(b). The surface roughness of a particle is able to lower the free energy barrier of embryo formation, thus we can expect that the particles with rougher surfaces requires lower degree of supersaturation for the water vapor to achieve heterogeneous condensation on their surfaces.

3.3. Nucleation rate

Nucleation rate represents the number of critical embryos created on a particle surface per second. Basically, the nucleation rate increases with supersaturation of the water vapor and size of the particle. Here we characterize the effect of particle surface roughness on the nucleation rate. The relationship between self-affine fractal factor $C_\alpha\sigma/\xi$ and nucleation rate J at different saturations of water vapor is plotted in Fig. 8. Self-affine fractal factor increasing from 0 to 0.1 results in rapid increase in nucleation rate. As mentioned above, surface roughness enhances wetting and decreases the local contact angle. Since nucleation rate is very sensitive with the change of contact angle, self-affine fractal factor contributes significantly to nucleation rate. This result leads us to conclude that the surface roughness favors the embryo formation on the $PM_{2.5}$ particles.

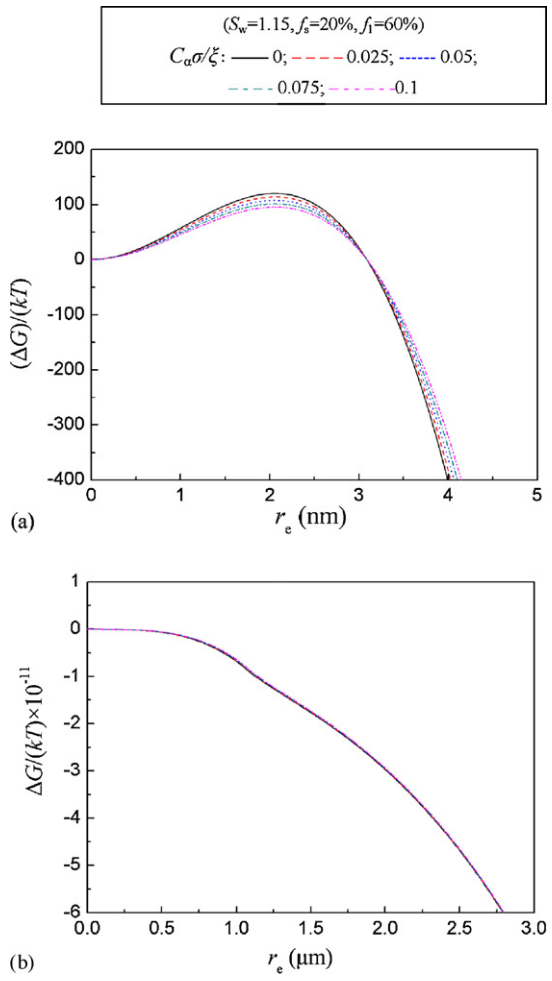

Fig. 7. Influence of self-affine fractal factor on free energy of embryo formation. (a) Initial stage of nucleation, (b) process of embryo growth.

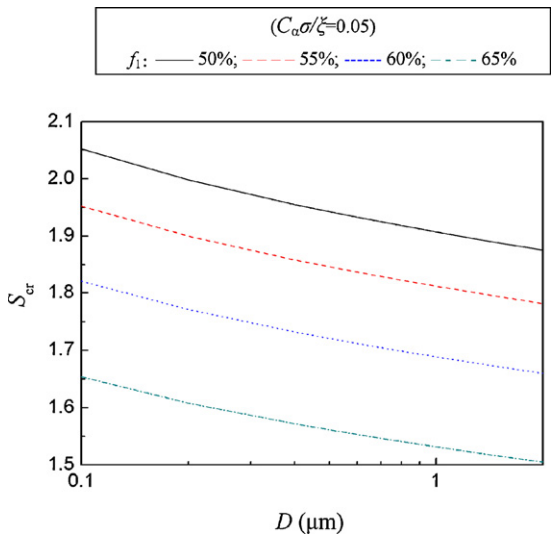

Fig. 9. Critical nucleation saturation at different mass fraction of $CaCl_2$ in soluble salts.

3.4. Critical nucleation saturation

The critical nucleation saturation is usually taken as the saturation for which the nucleation rate is $1\,s^{-1}$, if calculating the nucleation rate per particle using the classical theory of heterogeneous nucleation. Critical saturation indicates ambient saturation at which a particle will promote almost immediate nucleation and condensation. The creation of a suitable supersaturated vapor is essential to particle enlargement by heterogeneous condensation, and thus the determination of critical saturation is the key step to application of heterogeneous condensation for the removal of the $PM_{2.5}$ particles.

The present air pollution control equipments whose particulates capture efficiencies are higher than 90%, are generally less efficient in collecting particles less than 2.5 μm in size. In fact, the equipments have a collection efficiency minimum in the 0.1–1 μm size range [20]. Since our work focuses on $PM_{2.5}$ particles, we choose the

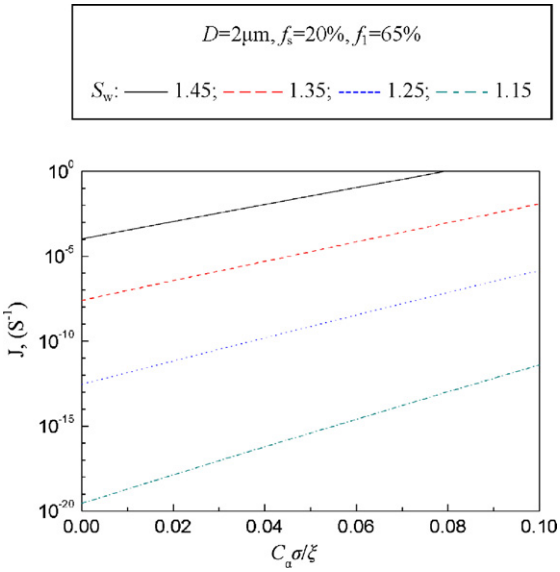

Fig. 8. Relationship between self-affine fractal factor and nucleation rate.

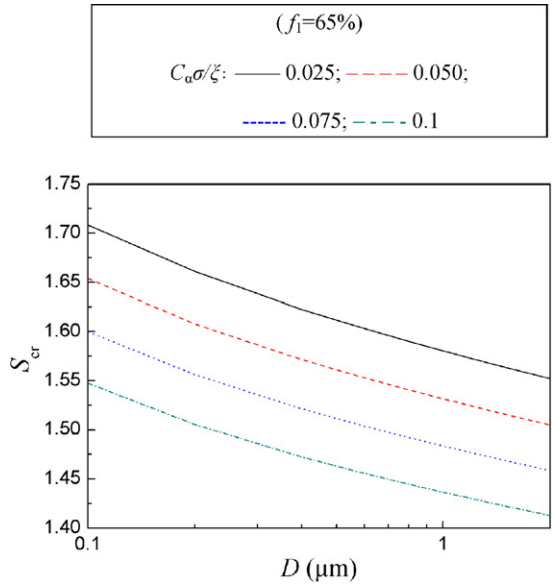

Fig. 10. Critical nucleation saturation at different self-affine fractal factor.

particles with insoluble core diameter ranging from 0.1 to 2 μm and calculate the critical saturation.

The dependences of the critical nucleation saturation S_{cr} on the diameter of the insoluble core D under different conditions are presented in Figs. 9 and 10. As the mass fraction of $CaCl_2$ f_1 varies from 50 to 65%, the critical saturation S_{cr} decreases 19.5%, as shown in Fig. 9. In another case, as the self-affine fractal factor $C_\alpha\sigma/\xi$ varies from 0.025 to 0.1, the critical saturation decreases and its variation amounts to 8.8%, as shown in Fig. 10. From the results in the two figures, S_{cr} is strongly affected by the particle size. A particle can be activated at saturations equal to higher than its critical saturation. Once the particle is activated, water vapor will condensate on it immediately and the particle will grow very rapidly by heterogeneous condensation until supersaturation disappears. The results also show that the degrees of critical saturations are too high for industrial applications. However, the theoretical model used in this study is still crude, further experiments are necessary to determine more reliable critical saturations.

4. Conclusions

In this paper an approach for calculating the characteristics of water vapor nucleation on the $PM_{2.5}$ from MSWI has been developed. The free energy of embryo formation, the nucleation rate and the critical nucleation saturation under different conditions were calculated, and the corresponding results were obtained.

Results show that the free energy barrier of embryo formation is not influenced by the total mass of soluble salts in the $PM_{2.5}$ when the mass fraction of each salt is constant. While the total mass of soluble salts does not change, the free energy barrier changes remarkably with the compositions of the soluble salts in the $PM_{2.5}$. It is also found that the free energy barrier of embryo formation decreases due to the surface roughness of the particle. Simulation results of the nucleation rate and the critical nucleation saturation indicate that both the compositions of the soluble salts and the surface roughness dominate the nucleation capabilities of the $PM_{2.5}$ from MSWI. This study gives the first indications of water vapor nucleation characteristics on the $PM_{2.5}$ from MSWI, further experimental studies are needed to develop more useful heterogeneous nucleation theories and to determine more reliable nucleation properties.

Acknowledgements

The authors gratefully acknowledge the support from the National Key Program of Basic Research in China (No. 2002CB211604) and the National Natural Science Foundation of China (No. 20576020).

References

[1] N. Englert, Fine particles and human health-a review of epidemiological studies, Toxicol. Lett. 149 (2004) 235–242.
[2] M.S. Zhang, Y. Song, X.H. Cai, A health-based assessment of particulate air pollution in urban areas of Beijing in 2000–2004, Sci. Total Environ. 376 (2007) 100–108.
[3] S. Van Der Zee, G. Hoek, H. Harssema, Characterization of particulate air pollution in urban and non-urban areas in the Netherlands, Atmos. Environ. 32 (1998) 3717–3729.
[4] J. Yoo, K. Kim, H. Jang, Emission characteristics of particulate matter and heavy metals from small incinerators and boilers, Atmos. Environ. 36 (2002) 5057–5066.
[5] S. Heidenreich, U. Vogt, H. Büttner, A novel process to separate submicron particles from gases—a cascade of packed columns, Chem. Eng. Sci. 55 (2000) 2895–2905.
[6] N.H. Fletcher, Size effect in heterogeneous nucleation, J. Chem. Phys. 29 (1958) 572–576.
[7] B. Gorbunov, R. Hamilton, Water nucleation on aerosol particles containing both soluble and insoluble substances, J. Aerosol Sci. 28 (1997) 239–248.
[8] B. Gorbunov, R. Hamilton, N. Clegg, Water nucleation on aerosol particles containing both organic and soluble inorganic substance, Atmos. Res. 47 (1998) 271–283.
[9] M. Lazaridis, Ø. Hov, K. Eleftheriadis, Heterogeneous nucleation on rough surfaces: implications to atmospheric aerosols, Atmos. Res. 55 (2000) 103–113.
[10] P.J. He, H. Zhang, Z.D. Wang, Pollution characteristics of air pollution control residues from municipal solid waste incineration plant, J. Tongji Univ. 31 (2003) 972–976.
[11] P.J. He, H. Zhang, Q.K. Cao, Characterization of APC residues from Shanghai Pudong waste-to-energy facility, Environ. Chem. 23 (2004) 38–41.
[12] P.J. Zhang, C.G. Zhang, H. Zhang, Pollution characteristics and management strategy of MSWI APC residues, Environ. Sanitation Eng. 12 (2004) 3–5.
[13] T.V. Subrahmanyam, M.B. Monte, A. Middea, et al., Contact angles of quartz by capillary penetration of liquid and captive bubble techniques, Miner. Eng. 12 (1999) 1347–1357.
[14] T.S. Chow, Noise and fluctuations of rough surfaces, Phys. Rev. Lett. 79 (1997) 1086–1089.
[15] T.S. Chow, Wetting of rough surfaces, J. Phys. Condens. Matter 10 (1998) L445–L451.
[16] Y.S. Liu, C.M. Xu, Y.F. Hu, Prediction of water activity for mixed aqueous solutions from the data of their binary constituent solutions, Chin. J. Chem. Eng. 12 (2004) 470–475.
[17] Y.F. Hu, H. Lee, Prediction of the surface tension of mixed electrolyte solutions based on the equation of Patwardhan and Kumar and the fundamental Butler equation, J. Colloid Interface Sci. 269 (2004) 442–448.
[18] H.R. Pruppacher, J.D. Klett, Microphysics of Clouds and Precipitation, Kluwer Academic Publishers, London, 1978.
[19] X.D. Wang, X.F. Peng, J.F. Lu, Contact angle hysteresis on rough solid surfaces, Heat Transfer-Asian Res. 33 (2004) 201–210.
[20] J.J. Helble, A model for the air emissions of trace metallic elements from coal combustors quipped with electrostatic precipitators, Fuel Process. Technol. 63 (2000) 125–147.